Chinese Chemical Letters 33 (2022) 757–761

Contents lists available at ScienceDirect

Chinese Chemical Letters

journal homepage: www.elsevier.com/locate/cclet

Enhanced oxidase-like activity of g-C_3N_4 nanosheets supported Pd nanosheets for ratiometric fluorescence detection of acetylcholinesterase activity and its inhibitor

Chenghui Zhang[a], Pengjuan Ni[a], Bo Wang[a], Wendong Liu[a], Yuanyuan Jiang[a], Chuanxia Chen[a,*], Jian Sun[b,*], Yizhong Lu[a,*]

[a] School of Materials Science and Engineering, University of Jinan, Ji'nan 250022, China
[b] State Key Laboratory of Electroanalytical Chemistry, Changchun Institute of Applied Chemistry, Chinese Academy of Sciences, Changchun 130022, China

ARTICLE INFO

Article history:
Received 12 May 2021
Revised 20 July 2021
Accepted 5 August 2021
Available online 11 August 2021

Keywords:
Oxidase-like activity
Ratiometric fluorescence
Acetylcholinesterase
g-C_3N_4 nanosheets
Pd nanosheets

ABSTRACT

The undesirable enzymatic activity of nanozymes under near neutral pH condition and the traditional single signal output always restrict the analytical application of nanozyme-based biosensors. Herein, graphitic carbon nitride nanosheets supported palladium nanosheets composite (Pd/g-C_3N_4) with both oxidase-like activity and fluorescent property is synthesized. Notably, Pd/g-C_3N_4 exhibits enhanced oxidase-like activity compared to Pd NSs under pH 7.4. By combining Pd/g-C_3N_4 with *o*-phenylenediamine (OPD), a ratiometric fluorescence assay for acetylcholinesterase (AChE) activity detection is developed. Pd/g-C_3N_4 can catalyze oxidation of nonfluorescent OPD to fluorescent oxidized OPD (oxOPD, Em = 565 nm), which can quench fluorescence of g-C_3N_4 supporter (Em = 441 nm) through fluorescence resonance energy transfer (FRET). However, in presence of AChE, acetylthiocholine can be hydrolyzed into thiocholine, which will block the oxidase-like activity of Pd/g-C_3N_4 and then hamper the FRET process. This ratiometric fluorescence assay is also viable to screen AChE inhibitor. This work will guide design of ratiometric fluorescence assay based on nanozymes with improved enzymatic activity.

Acetylcholinesterase (AChE), an acetylcholine (ACh) hydrolase, plays a vital role in determining the contents of ACh that participates in learning and memory processes [1]. Low ACh level will cause Alzheimer's disease (AD) [2]. As for AD, some inhibitors, such as tacrine, are used to clinically treat AD by restraining activity of AChE [3]. So, it is significantly important to develop reliable and simple methods for AChE activity detection and inhibitors screening. To date, many efforts have been dedicated to colorimetry [4], fluorometry [5], electrochemistry [6], chemiluminescence [7]. Among them, fluorometry holds distinct advantages for its simplicity and sensitivity [8,9]. However, conventional fluorometric assays based on the single signal output are inevitably disturbed by various objective conditions. By comparison, ratiometric fluorescent method based on self-calibration of double signals has been proved to give more reliable results [10-15].

Nanozymes are believed to have lower cost with convenient preparation process and higher stability than natural enzymes [16]. To date, several kinds of nanomaterials, including noble metals [17], metal oxides [18] and so on [19-21] have been proved to exhibit enzymatic activities. Among them, noble metals-based nanozymes have attracted great interesting due to their good stability [17]. To this end, ultrathin two-dimensional (2D) noble metal nanosheets (NSs) with high ratio of surface to volume have become a hot research topic in fields of sensing and catalysis, benefiting from their smaller diffusion barrier and more accessible active sites for substrates, compared to their 3D counterparts [22-24]. Unfortunately, like other nanozymes, though exhibit good activity under acidic condition, the activity of noble metal-based nanozymes is significantly decreased under near neutral pH condition, which is inconvenient in practical applications. So, it is meaningful to develop efficient method to enhance enzymatic activity of noble metal, especially under physiological pH condition.

It is well known that the catalytic performance of metal catalysts can be facilely improved by loading them onto appropriate supporters [25]. Among various supporters, graphitic carbon nitride nanosheets (g-C_3N_4 NSs) have attracted enormous attention in bio-sensing filed due to their easy preparation and good biocompatibility [10]. Besides, g-C_3N_4 NSs with intrinsic π electronic structure and abundant nitrogen sites can enrich some reactants through π-π stacking and/or hydrogen bonding interac-

* Corresponding authors.
E-mail addresses: mse_chencx@ujn.edu.cn (C. Chen), jiansun@ciac.ac.cn (J. Sun), mse_luyz@ujn.edu.cn (Y. Lu).

https://doi.org/10.1016/j.cclet.2021.08.017
1001-8417/

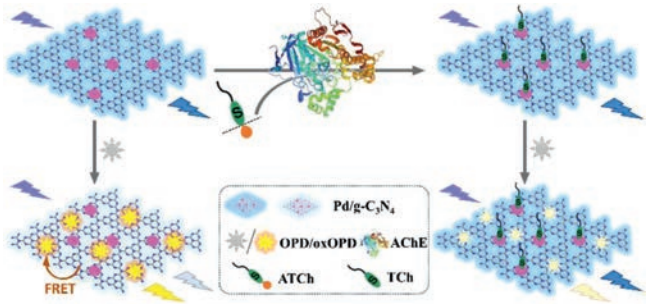

Scheme 1. Illustration of the Pd/g-C_3N_4 based ratiometric fluorescence strategy for determination of AChE activity.

tions, which will shorten the distance between reactants and catalytic sites supported on g-C_3N_4 NSs [23]. Moreover, the fluorescence property of g-C_3N_4 NSs displays great potential to construct ratiometric fluorescence assay [26-28]. Hence, developing composites by supporting the 2D noble metals NSs on g-C_3N_4 NSs will be expectable to construct ratiometric fluorescence assay.

Herein, a neoteric Pd/g-C_3N_4 composite possessing both efficient oxidase-like activity and fluorescent property is synthesized. Notably, the oxidase-like activity of Pd NSs is successfully enhanced under neutral pH condition after loaded onto g-C_3N_4 NSs. By combining Pd/g-C_3N_4 with *o*-phenylenediamine (OPD), a ratiometric fluorescence assay is developed for AChE activity detection with acetylthiocholine (ATCh) as substrate (Scheme 1). Pd/g-C_3N_4 as oxidase mimic can catalyze the transformation of nonfluorescent OPD to fluorescent oxidized OPD (oxOPD, 2,3-diaminophenazine). Then the fluorescence of g-C_3N_4 NSs supporter is quenched by oxOPD through fluorescence resonance energy transfer (FRET). However, in presence of AChE, ATCh is hydrolyzed into thiocholine (TCh), which poisons the active sites by forming Pd-S bond and blocks the Pd/g-C_3N_4 catalyzed OPD oxidation. Thus, the fluorescence of oxOPD is weakened and fluorescence of Pd/g-C_3N_4 is recovered, providing a ratio signal for AChE detection. Furthermore, tacrine is detected as a proof-of-concept to investigate the AChE inhibitor screening ability of this ratiometric fluorescence assay.

Firstly, Pd NSs is synthesized by reducing palladium(II) acetylacetonate in presence of tungsten hexacarbonyl ($W(CO)_6$), which can produce CO, serving as capping and reducing agent [29]. Secondly, melamine is pyrolyzed to give bulk g-C_3N_4, which is refluxed by HNO_3, followed by ultrasonic exfoliated to produce g-C_3N_4 NSs [26]. Lastly, Pd/g-C_3N_4 is obtained by mixing aqueous solution of Pd NSs and g-C_3N_4 NSs under stirring. Transmission electron microscopy (TEM) shows that hexagonal Pd NSs are obtained with a lateral diameter of *ca.* 8.44 nm and an average thickness of *ca.* 1.0 nm (Fig. 1a and Fig. S1 in Supporting information). Fig. S2 (Supporting information) indicates that g-C_3N_4 NSs are multiple layers with thickness of below 7.0 nm. And the obtained g-C_3N_4 NSs have better dispersibility in water than bulk g-C_3N_4 (Fig. S3 in Supporting information), which is beneficial for bioanalysis. As shown in Fig. 1b, Pd NSs are successfully deposited on the surface of g-C_3N_4 NSs without changing both of their morphologies.

As for Pd NSs, X-ray diffraction (XRD) pattern shows two weak diffraction peaks centered at 40.42° and 68.34°, which are ascribed to (111) and (220) planes of Pd (JCPDS-46-1043), demonstrating the cubic structure of Pd NSs (Fig. 1c). Similar to other Pd NSs synthesized in presence of $W(CO)_6$ [22], the obtained Pd NSs show lower crystallinity compared to those obtained by direct filling CO [30]. For bulk g-C_3N_4, there are one strong peak centered at 27.70° and one weak peak centered at 13.34°, which are assigned to the typical (002) plane of inter-planar stacking in graphitic-like materials and (100) plane of in-plane structural packing motif among the sheets, respectively (Fig. 1c) [31,32]. Comparatively, the intensity of peak ascribed to (002) plane decreases accompanied with shifting from 27.70° to higher degree of 27.82°, whereas the weak peak corresponding to (100) plane disappears in g-C_3N_4 NSs, suggesting that bulk g-C_3N_4 is successfully exploited into nanoscale layers after acidic treatment and ultrasonic exfoliation (Fig. 1c and Fig. S4 in Supporting information) [27]. However, no obvious peak of Pd is found in Pd/g-C_3N_4 due to the low loading content (4.03 wt%) and undesirable crystallinity of Pd NSs (Fig. 1c) [22]. In addition, Pd/g-C_3N_4 exhibits similar diffraction patterns to g-C_3N_4 NSs, suggesting that the loading of Pd NSs does not disturb the structure of g-C_3N_4 NSs, which is also confirmed by the similar Fourier transform infrared characteristic peaks of g-C_3N_4 NSs and Pd/g-C_3N_4 (Fig. S5 in Supporting information).

X-ray photoelectron spectroscopy (XPS) measurements are conducted to further disclose chemical composition of those materials. Compared to g-C_3N_4 NSs that contain C, N, and O peaks, a new peak arising from Pd is found in Pd/g-C_3N_4 (Fig. S6 in Supporting information). Taken TEM images of Pd/g-C_3N_4 in mind, the existence of Pd peak further demonstrate that Pd NSs are successful supported onto g-C_3N_4 NSs. The high-resolution XPS spectra of Pd 3d, C 1s, and N 1s are analyzed. For Pd in Pd/g-C_3N_4, the resolved peaks located at 335.7 and 340.9 eV are attributable to Pd^0 $3d_{5/2}$ and Pd^0 $3d_{3/2}$, while the other pair of peaks centered at 337.6 and 343 eV originate from Pd^{2+} $3d_{5/2}$ and Pd^{2+} $3d_{3/2}$, respectively (Fig. 1d) [23]. The C 1s peak can be divided into four peaks centered at 284.7, 286.2, 287.9, and 288.5 eV, ascribing to graphitic carbon (C-C), sp^3-hybridized carbon with oxygen (C-O), sp^2-hybridized carbon with nitrogen (N-C=N), and oxygen (C=O), respectively (Fig. 1e) [33,34]. The N 1s spectrum is deconvolved into four peaks, in which the binding energies at 398.5, 399.7, and 400.9 eV are assigned to the sp^2-hybridized nitrogen (C-N=C) in triazine ring, the tertiary nitrogen HN–$(C)_2$, and N–$(C)_3$ groups, respectively. While the relative weaker and broad peak centered at 404.1 eV belongs to the quaternary nitrogen, arising from the positive charge localization and/or delocalization of π electron in the heterocycles (Fig. 1f) [33,34]. No obvious shifting of binding energy of N 1s can be found in Pd/g-C_3N_4 in comparison with g-C_3N_4 NSs, excluding the possibility that Pd NSs attach on g-C_3N_4 NSs *via* Pd-N chemical bond [23]. Furthermore, zeta potentials of Pd NSs and g-C_3N_4 NSs dispersed in ultrapure water are measured to be –13.9 and 15.2 mV (Fig. S7 in Supporting information), suggesting that there exists electrostatic interaction between them. These results demonstrate that Pd/g-C_3N_4 composites are successfully obtained based on electrostatic interaction between Pd NSs and g-C_3N_4 NSs.

The oxidase-like activities of Pd NSs, g-C_3N_4 NSs and Pd/g-C_3N_4 are examined by the catalytic oxidation of OPD under pH 7.4 that is similar to physiological environment. As depicted in Fig. 2a, both Pd NSs and Pd/g-C_3N_4 can trigger the oxidation of colorless OPD to orange with corresponding absorption peaks at 419 nm. In contrast, the control solution with g-C_3N_4 NSs shows no color change, indicating that it is Pd NSs rather than g-C_3N_4 NSs that exhibit oxidase-like activity toward catalytic oxidation of OPD to oxOPD. Despite its inactive when exist alone, g-C_3N_4 NS effectually strengthen the catalytic activity of Pd NSs. As proof, the absorbance of Pd/g-C_3N_4 + OPD is higher (about 1.43 times) than that of Pd NSs + OPD. To probe into the enhancement mechanism, steady-state kinetic parameters including Michaelis constant (K_m) and maximal reaction rate (V_{max}) are calculated from typical Michaelis-Menten curves of Pd/g-C_3N_4 and Pd NSs. As shown in Fig. 2b, the K_m of Pd/g-C_3N_4 (0.086 mmol/L) is lower than that of Pd NSs (0.121 mmol/L), indicating Pd/g-C_3N_4 show higher affinity for OPD. Meanwhile, the V_{max} of Pd/g-C_3N_4 is higher than that of Pd NSs, further revealing Pd/g-C_3N_4 has enhanced catalytic efficiency compared to Pd NSs. This result can be explained by the fact that g-C_3N_4 NSs can adsorb OPD *via* π-π stacking and hy-

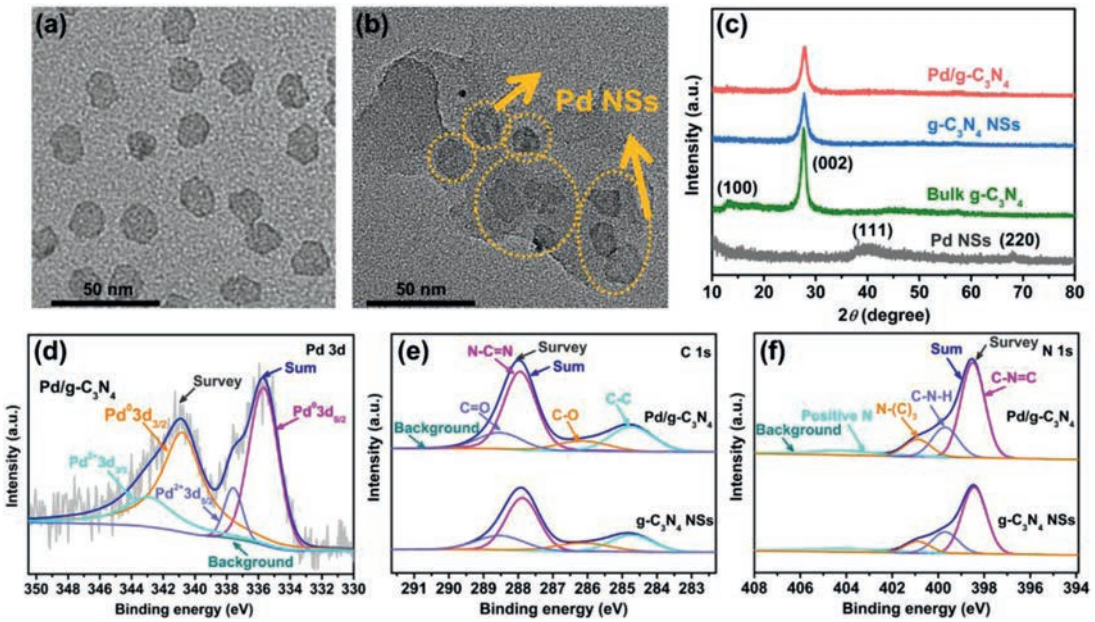

Fig. 1. TEM images of (a) Pd NSs and (b) Pd/g-C_3N_4. (c) XRD patterns and high-resolution XPS spectra of (d) Pd 3d, (e) C 1s, (f) N 1s.

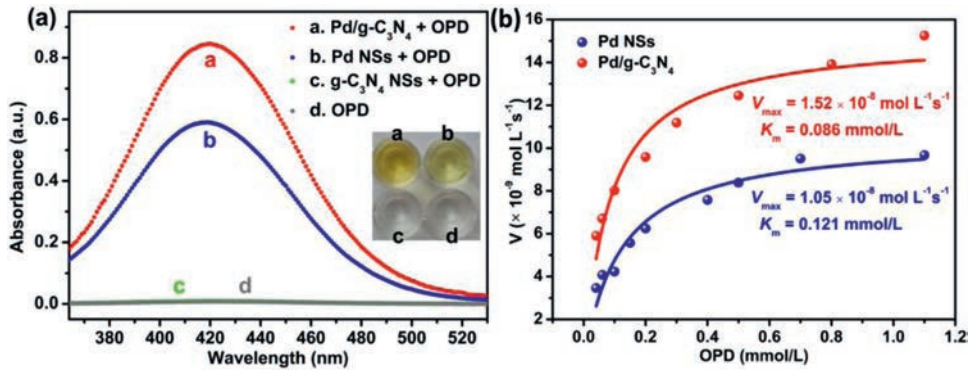

Fig. 2. UV-vis absorption spectra and the corresponding color change of OPD oxidation catalyzed by Pd NSs, Pd/g-C_3N_4 or g-C_3N_4. (b) Michaelis-Menten kinetics for the oxidation of OPD.

drogen bonding interaction, endowing higher concentration of OPD near to Pd NSs supported on g-C_3N_4 NSs, resulting Pd/g-C_3N_4 with enhanced catalytic activity toward OPD oxidation [23].

To reveal the origin of catalytic activity of Pd NSs as oxidase mimics, the absorbance of Pd NSs + OPD system in O_2/air/N_2-saturated solutions are explored. Those results show that the catalytic activity of Pd NSs in different atmosphere is in the order of O_2 > air > N_2 (Fig. S8a in Supporting information), indicating that O_2 plays vital role for Pd NSs as oxidase mimics. During this reaction process, O_2 might be activated to generate several reactive oxygen species including superoxide anion ($O_2^{\bullet-}$), singlet oxygen ($^1O_2$), hydroxyl radicals ($^\bullet$OH) [35]. Initially, the reactive oxygen species are determined based on scavenger mechanism with superoxide dismutase (SOD), tryptophan, and isopropanol as scavengers for $O_2^{\bullet-}$, $^1O_2$, and $^\bullet$OH, respectively [36,37]. From Fig. S8b (Supporting information), isopropanol has little effect on Pd NSs-catalyzed OPD oxidation, suggesting $^\bullet$OH is not involved in this reaction. Whereas, as the concentration of SOD and tryptophan increased, the absorbance is gradually decreased, indicating that $O_2^{\bullet-}$ and $^1O_2$ are all produced. In addition, electron paramagnetic resonance (EPR) spectra also prove that no signal of $^\bullet$OH can be found (Fig. S8c in Supporting information). However, the four peaks with intensity of 1:1:1:1 corresponding to $O_2^{\bullet-}$ and the triplet peaks ascribing to $^1O_2$ all present in EPR spectra (Figs. S8d and e in Supporting information). The above phenomena display that Pd NSs can activate the dissolved O_2 into $O_2^{\bullet-}$ and $^1O_2$, which is responsible for OPD oxidation.

Pd/g-C_3N_4 exhibits abroad excitation band ranging from 306 to 410 nm (Fig. S9 in Supporting information) and a fluorescence emission peak centered at 441 nm upon exciting at 390 nm (Fig. S10a in Supporting information). And a new peak centered at 565 nm derived from oxOPD is recorded when OPD is introduced, whereas the intensity of peak centered at 441 nm is significantly decreased. This phenomenon indicates that oxOPD not only emits fluorescence but also quenches fluorescence of g-C_3N_4 supporter, which provides basis for developing ratiometric fluorescence assay. Then the quenching mechanism of oxOPD toward g-C_3N_4 supporter is investigated. From Fig. S10b (Supporting information), an obvious overlap between the emission spectrum of Pd/g-C_3N_4 and the absorption spectrum of oxOPD is found, suggesting the existence of FRET and/or inner-filter effect between Pd/g-C_3N_4 and oxOPD [15]. Furthermore, the fluorescence lifetime of Pd/g-C_3N_4 decays from 4.0 ns to 1.8 ns (Fig. S10c in Supporting information), and the zeta potential of Pd/g-C_3N_4 changes from –6.9 mV

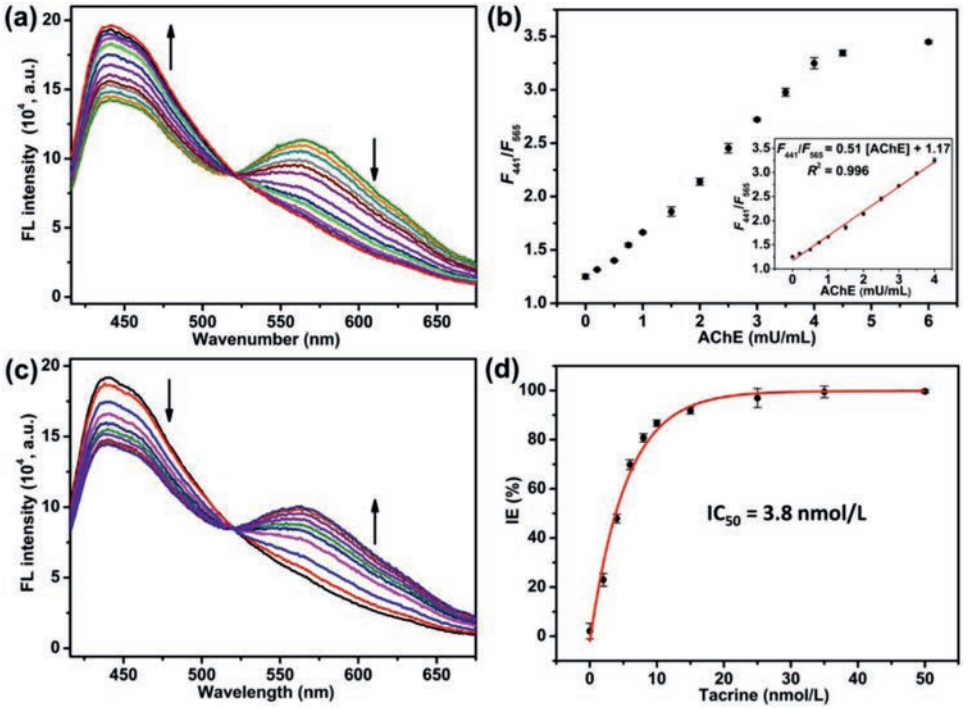

Fig. 3. (a) Fluorescence emission spectra of Pd/g-C_3N_4 + OPD system toward various AChE activities. (b) The plot of F_{441}/F_{565} as a function of AChE activity (the inserted graph is the liner response to AChE activity). (c) Fluorescence emission spectra of Pd/g-C_3N_4 + OPD system with ATCh (30 μmol/L), AChE (6 mU/mL) and different concentrations of tacrine. (d) The IE plot of tacrine toward AChE as a function of tacrine concentrations.

to –4.9 mV after incubation with OPD (Fig. S10d in Supporting information). All of those above results disclose an electrostatic interaction-based FRET process between positively charged oxOPD and negatively charged Pd/g-C_3N_4.

It is known that thiols tend to coordinate with metal atoms [38], thus can tailor the enzymatic activity of Pd NSs. L-Cysteine (Cys) is selected as mercapto molecule to verify the interaction between Pd NSs and thiols. Compared to Cys, XPS curve of S 2p in Pd NSs + Cys shows a new peak with higher binding energy, proving that there exists strong coordination interaction between Pd NSs and Cys (Fig. S11 in Supporting information). Besides, the electrocatalytic oxygen reduction reaction of Pd NSs is immediately inhibited upon addition of Cys, further indicating the interaction between Pd NSs and Cys (Fig. S12 in Supporting information) [21]. So, it is reasonably believed that the active sites of Pd NSs can be blocked by forming Pd-S bond upon addition of thiols, thus inhibiting the oxidase-like activity of Pd NSs. As further proved, the absorbance of Pd NSs + OPD system gradually decreases accompanying the increased contents of Cys. And the calculated variation of absorbance shows a good linearly correlated with Cys concentration ranging of 1-15 μmol/L (Fig. S13 in Supporting information).

Inspired by such phenomenon, a ratiometric fluorescence strategy for AChE is proposed by taking ATCh as substrate (Scheme 1). From Fig. S14 (Supporting information), Pd/g-C_3N_4 + OPD system shows no significant change with individual ATCh or AChE. However, in presence of AChE, ATCh can be transformed into thiol-containing TCh, which inhibits the oxidase-like activity of Pd/g-C_3N_4 by forming Pd-S bond. As a result, the oxidation of OPD and the subsequent FRET process are impeded, accompanied with the weakened and recovered fluorescence of oxOPD (Em = 565 nm) and Pd/g-C_3N_4 (Em = 441 nm), respectively. Therefore, the quantitative determination of AChE activity through change of F_{441}/F_{565} can be realized.

In order to realize satisfactory detection performance, the loading amount of Pd NSs; the needed time for hydrolysis of AChE into ATCh and the oxidation of OPD into oxOPD; the concentration of ATCh, OPD, and Pd/g-C_3N_4; the pH and temperature of Pd/g-C_3N_4 catalyzed oxidation of OPD, are all explored in detail to give optimal sensing parameters (Figs. S15-S17 in Supporting information). Additionally, to ensure the accuracy and reproducibility of this dissolved oxygen-dependent sensing system, all experiments are performed under the same temperature, atmospheric pressure and salt concentration. Then, under the optimal sensing condition, the AChE activity detection is performed. As expected, the emission intensity at 441 nm of Pd/g-C_3N_4 is gradually increased, while the emission intensity at 565 nm of oxOPD is gradually decreased upon the increased AChE activity ranging from 0.2 mU/mL to 6 mU/mL (Fig. 3a). Meanwhile, the value of F_{441}/F_{565} increases accompanied with increased AChE activity (Fig. 3b). The linear dependence relationship (R^2 = 0.996) with AChE activity ranging from 0.2 mU/mL to 4.0 mU/mL is realized (Fig. 3b). The detection limit of 0.06 mU/mL ($3\sigma/S$) is comparable to or even lower than previously reported AChE activity assays (Table S1 in Supporting information).

To assess anti-interference performance and selectivity of this assay, some biomolecules and common ions, including α-glucosidase, glucose oxidase, pepsin, lysozyme, pancreatin, bull serum albumin, trypsin, D-glucose, L-aspartic, glycine, L-alanine, L-leucine, Ca^{2+}, K^+, Mg^{2+} and NO_3^- are selected as interferents. The results in Fig. S18 (Supporting information) indicate that those potential interferents show no significant influence on this ratiometric fluorescence assay either with or without AChE, suggesting good anti-interference performance and high selectivity toward AChE of this assay, which is due to the specificity of AChE toward its substrate. Furthermore, the feasibility of this ratiometric fluorescence assay is investigated by detecting AChE activity in human serums. The human serum samples were provided by the Hospital of University of Jinan (Ji'nan, China) and obtained from healthy donors. Besides, all experiments were approved by the Life-Science Ethics Review Committee of University of Jinan and obtained the

informed consent from the blood donors of this project. The interferences from biothiols in serums are negligible (Fig. S19 in Supporting information), or can be eliminated by *N*-ethylmaleimide [15]. Acceptable recoveries and relative standard deviation within the ranges of 99.0%–108.3% and 0.80%–3.40% are achieved, respectively (Table S2 in Supporting information), indicating this ratiometric fluorescence assay is suitable for detecting AChE activity in real samples.

To further develop potential application to inhibitor screening of this ratiometric fluorescence assay, tacrine, an unequivocable AChE inhibitor used in AD therapy, is selected as a model to assess the inhibitory activity assay. Feasibility analysis demonstrates that tacrine puts no effect on the oxidase-like activity of Pd/g-C_3N_4 (Fig. S20 in Supporting information). With the concentration increase of tacrine, the fluorescence emissions centered at 441 nm and 565 nm are gradually decreased and increased, respectively, indicating that the activity of AChE is successfully inhibited by tacrine (Fig. 3c). By using the plot of inhibition efficiency (IE) as function of tacrine concentration (Fig. 3d), IC_{50} value, the needed concentration of tacrine for the inhibition of 50% enzyme activity, is obtained to be 3.8 nmol/L, which is similar to previous literatures [39,40].

In summary, Pd/g-C_3N_4 nanocomposite with enhanced oxidase-like activity compared to Pd NSs under pH 7.4 is successfully synthesized. By combining the obtained Pd/g-C_3N_4 composite with OPD, a sensitive and selective ratiometric fluorescence platform is developed for AChE activity determination. This strategy is suitable for serology test benefitting from the reliable signal output. Moreover, this method is feasible to screen AChE inhibitor. Look forward to the future, such ratiometric fluorescent assay can be extended to monitoring other thiol-containing species and thiol-generating or consuming biological process. This work demonstrates a novel guidance for designing nanozymes with improved activity in biosensing system, especially under physiological pH condition.

Declaration of competing interest

The authors declare that they have no known competing financial interests or personal relationships that could have appeared to influence the work reported in this paper.

Acknowledgments

This work was supported by the Natural Science Foundation of Shandong Province (Nos. ZR2020QB033 and ZR2019YQ10), the National Natural Science Foundation of China (Nos. 21904048, 21974132, 21902061 and 21902062) and the Young Taishan Scholars Program (No. tsqn201812080).

Supplementary materials

Supplementary material associated with this article can be found, in the online version, at doi:10.1016/j.cclet.2021.08.017.

References

[1] H. Soreq, S. Seidman, Nat. Rev. Neurosci. 2 (2001) 294–302.
[2] N.C. Inestrosa, A. Alvarez, C.A. Pérez, et al., Neuron 16 (1996) 881–891.
[3] C. Lei, Z. Wang, Z. Nie, et al., Anal. Chem. 87 (2015) 1974–1980.
[4] L. Huang, D.W. Sun, H. Pu, et al., Sens. Actuator. B: Chem. 290 (2019) 573–580.
[5] J. Sun, X. Yang, Biosens. Bioelectron. 74 (2015) 177–182.
[6] D. Du, W. Chen, J. Cai, et al., J. Electroanal. Chem. 623 (2008) 81–85.
[7] S. Sabelle, P.Y. Renard, K. Pecorella, et al., J. Am. Chem. Soc. 124 (2002) 4874–4880.
[8] C. Chen, J. Zhao, Y. Lu, J. Sun, X. Yang, Anal. Chem. 90 (2018) 3505–3511.
[9] C. Fan, X. Lv, F. Liu, et al., ACS Sensors 3 (2018) 441–450.
[10] W. Deng, Y. Peng, H. Yang, et al., ACS Appl. Mater. Interfaces 11 (2019) 29072–29077.
[11] M. Ye, B. Lin, Y. Yu, et al., Microchim. Acta 187 (2020) 511.
[12] C.Y. Ke, Y.T. Wu, W.L. Tseng, Biosens. Bioelectron. 69 (2015) 46–53.
[13] X. Xu, Y. Cen, G. Xu, et al., Biosens. Bioelectron. 131 (2019) 232–236.
[14] R. Ma, M. Xu, C. Liu, et al., ACS Appl. Mater. Interfaces 12 (2020) 42119–42128.
[15] M. Wang, L. Liu, X. Xie, et al., Sens. Actuators B: Chem. 313 (2020) 128023.
[16] H. Wei, E. Wang, Chem. Soc. Rev. 42 (2013) 6060–6093.
[17] J. Wei, X. Chen, S. Shi, S. Mo, N. Zheng, Nanoscale 7 (2015) 19018–19026.
[18] L. Gao, J. Zhuang, L. Nie, et al., Nat. Nanotechnol. 2 (2007) 577–583.
[19] K. Fan, J. Xi, L. Fan, et al., Nat. Commun. 9 (2018) 1440.
[20] I. Nath, J. Chakraborty, F. Verpoort, Chem. Soc. Rev. 45 (2016) 4127–4170.
[21] Y. Wu, L. Jiao, X. Luo, et al., Small 15 (2019) 1903108.
[22] Y. Tang, P. Zhou, Y. Chao, et al., Sci. China Mater. 62 (2019) 351–358.
[23] K. Gu, X. Pan, W. Wang, et al., Small 14 (2018) 1801812.
[24] C. Chen, W. Liu, P. Ni, et al., ACS Appl. Mater. Interfaces 11 (2019) 47564–47570.
[25] X.H. Li, X. Wang, M. Antonietti, Chem. Sci. 3 (2012) 2170–2174.
[26] X. Wang, L. Qin, M. Lin, H. Xing, H. Wei, Anal. Chem. 91 (2019) 10648–10656.
[27] L. Wang, F. Zhu, S. Liao, et al., Talanta 197 (2019) 422–430.
[28] Z. Zhang, Y. Gao, P. Li, et al., Chin. Chem. Lett. 31 (2020) 2725–2729.
[29] Y. Li, Y. Yan, Y. Li, et al., CrystEngComm 17 (2015) 1833–1838.
[30] L. Chen, L.R. Zhang, L.Y. Yao, et al., Energy Environ. Sci. 12 (2019) 3099–3105.
[31] S. Zhou, Y. Liu, J. Li, et al., Appl. Catal. B: Environ. 158-159 (2014) 20–29.
[32] X. Wang, K. Maeda, A. Thomas, et al., Nat. Mater. 8 (2009) 76–80.
[33] L. Zhang, N. Ding, J. Wu, et al., Catal. Sci. Technol. 8 (2018) 3846–3852.
[34] Y.L.T. Ngo, W.M. Choi, J.S. Chung, S.H. Hur, Sens. Actuators B: Chem. 282 (2019) 36–44.
[35] L. Nana, L. Ruiyi, W. Qinsheng, et al., J. Hazard. Mater. 415 (2021) 125752.
[36] J. Liu, L. Meng, Z. Fei, P.J. Dyson, L. Zhang, Biosens. Bioelectron. 121 (2018) 159–165.
[37] H.H. Deng, X.L. Lin, Y.H. Liu, et al., Nanoscale 9 (2017) 10292–10300.
[38] W. Li, X. Sun, X. Zhao, et al., Chin. Chem. Lett. 31 (2020) 2473–2477.
[39] D. Zhao, C. Chen, J. Sun, X. Yang, Analyst 141 (2016) 3280–3288.
[40] P. Ni, Y. Sun, S. Jiang, et al., Sens. Actuator. B: Chem. 240 (2017) 651–656.